MDPI

Article

Title

Jorge Tarango-Yong [1,†,‡], Mario Rodríguez-Martínez [1,‡] and Raul Gutiérrez-Zalapa [2,*]

[1] Affiliation 1; e-mail@e-mail.com
[2] Affiliation 2; e-mail@e-mail.com
* Correspondence: e-mail@e-mail.com; Tel.: (optional; include country code; if there are multiple corresponding authors, add author initials) +xx-xxxx-xxx-xxxx (F.L.)
† Current address: Affiliation 3
‡ These authors contributed equally to this work.

Abstract: A single paragraph of about 200 words maximum. For research articles, abstracts should give a pertinent overview of the work. We strongly encourage authors to use the following style of structured abstracts, but without headings: (1) Background: place the question addressed in a broad context and highlight the purpose of the study; (2) Methods: describe briefly the main methods or treatments applied; (3) Results: summarize the article's main findings; (4) Conclusion: indicate the main conclusions or interpretations. The abstract should be an objective representation of the article, it must not contain results which are not presented and substantiated in the main text and should not exaggerate the main conclusions.

Keywords: keyword 1; keyword 2; keyword 3 (List three to ten pertinent keywords specific to the article; yet reasonably common within the subject discipline.)

1. Introduction

The Earth's magnetic field represents a final obstacle to the Solar Wind (SW) flux. When descelerated and defected by a non colisional shock wave in the flux direction, generates a cavity known as magnetosphere [1]. Since the Earth is embedded in this SW flux, is known that under adequated physical conditions (e.g magnetic reconnection) may exist some coupling between the magnetosphere and the Earth's ionosphere [2,3].

The Sun plays an important role in the physical proccesses that occur in the terrestrial magnetosphere-ionosphere system. When the SW interacts with the Earth's magnetosphere, particles may permeate the internal region via magnetic reconnection and penetrate to polar zones and generate boreal or austral auroras thus altering the system [4,5]. By the other hand, the Extreme Ultraviolet Radiation (EUV) and X-rays coming from the Sun may interact with the neutral atmoshere via photoionization [6]. However, in both cases the final result is that the ionosphere's free electrons population is altered.

Some Ionospheric Perturbations (IP) become relevant due to their spatial and temporal scale in the Space Weather scenario. At intermediate latitudes, the most common in the ionosphere are known as Traveling Ionospheric Disturbances (TIDs). Typically they divide into two groups: a) large scale TIDs, associated with geomagnetic storms with sizes of $\sim$2000 km, periods of $\sim$1 h and velocities of $\sim$700 km s^{-1}, and b) Medium-scale TIDs, which are not fully associated with geomagnetic storms, present sizes of $\sim$100 km, periods from 10 minutes to 1 hour and velocities between 50 km s^{-1} and 1×10^2 km s^{-1} [7]. Diverse methods have benn used to study TIDs, such as incoherent dispersion radars, high frequency Doppler emmisors, data from Global Positioning System (GPS) stations or even radiotelescopes like the VLA or the Mexican Array Radio Telescope (MEXART) [8,9].

On the other side, the Earth's ionosphere may be affected or modified by other proccesses, particularly there are studies that show how the Vetical Total Electron Content (vTEC) due to shock waves generated for rockets launched to space [10]. Similar proccesses modify the Earth's ionosphere due to objects entering the athmosphere from space, such as meteoroids like the one which fell on Chelyabinsk at 2013 [11]. Previously, the ionospheric

Citation: Tarango-Yong, J.; Rodríguez-Martínez, M.; Gutiérrez-Zalapa, R. Title. *Atmosphere* **2022**, *1*, 0. https://doi.org/

Received:
Accepted:
Published:

perturbations produced by this object were studied using two independent methods: a) detecting vTEC pertubations using GPS station near the impact location. And b) a wavelets analysis for detection of ...

In 2020 a meteoroid passed in mexican territory through mexican territory, which also was studied [12]. The meteoroid was recorded with outdoor cameras in different locations. The trajectory could be estimated, as well as other physical parameters.

In this work we will show a similar analysis for a sample of meteoroids detected in mexican territory by different methods. The first subsample consists in objects detected by the Geostationary Lightning Mapper (GLM) whose sizes are estimated between a few decimeters to meters in diameter [13–15]. The second subsample will consist in objects detected by ocular witnesses from the American Meteor Society and as comparisson we will include the morelian meteoroid reported in Sergeeva *et al.* [12] and the Chelyabinsk event Yang *et al.* [11]. The paper is arranged in the following way: §**??** describes the samples of meteoroids as well of the properties that can be obtained from direct observations. Also describes the GPS data corresponding to the dates and locations where each object was located. §**??** shows physical parameters of meteoroids obtained from the observed heights and energies. Finally, section §**??** shows the vTEC maps and scintillation indices obtained from GPS observations.

2. Methodology

2.1. Meteors Databases

We selected a sample of meteors which were observed in mexican territory from the Geostationary Lightning Mapper [13]. Originally this project was designed to detect lightning activity in earth's atmosphere, but has been proven that also can detect bolides entering the atmosphere. The detection comes from two satellites called GOES-16 and GOES-17 orbiting the earth in geostationary orbits. We used the interactive database available at https://neo-bolide.ndc.nasa.gov/#/. These data are publicly available and easily downloaded from the same website. For each event we can obtain the recorded trajectory of meteors and the corresponding light curve. The GLM satellites have an umbral magnitude for detection of -14. At this magnitude, a meteor is considered a bolide, and is expected to be at least decimeter-sized (in diameter) to reach such brightness. In the other hand, too bright meteors will saturate the detectors, and thus, lowering the quality of data. The result of this factors implies that the range in size of the objects in our sample should vary in diameter between decimeter to meter size. Each event also has assigned a confidence ratio, from low confidence to high, depending in how bright is the event itself and if the trajectory recorded by GLM ressembles a straight line. We chose only events whose confidence ratio is high, in order to be sure we chose the brightest objects, and thus, in the diameter size of bolides, we favored the meter-sized ones. In table 1 we list the object we chose to do this work, order in chronological order. GOES-16 and GOES-17 systematically detect the meteors at slightly different positions and at slightly different times, so we calculated the mean of the duration, latitude and longitude reported by both satellites for each event, and used the standard deviation as the uncertainties. In figure 1 we show the actual positions at which each bolide was detected.

From table 1 is also clear that the duration of all the bolides detection last less than a second. This observation suggests that the bolides remain undetected by the GLM satellites until they get fragmented due to stagnation pressure when they release a huge amount of energy and thus they become detectable.

By the other hand, we got another sample of 10 bolides from US Goverment (USG) sensors from the Center for Near Earth Object Studies (CNEOS), publicly available at https://cneos.jpl.nasa.gov/fireballs/, where we may obtain directly data about bolides position, the date and time each bolide was detected, the energy released at fragmentation, the velocity and the height (the last two not available for all bolides). As seen in table 2, the time span is quite larger, and the released energy is generally larger. Some elements appear in both samples, since are bright enough to be detected regardless the project involved. In

Table 1. List of bolides detected in mexican territory (plus one detected near Venezuela and one detected near Cuba), detected by the Geostationary Lighning mapper. The events are listed in chronological order. The listed duration, latitude and longitude correspond to the mean of the measurements of both GOES satellites. The uncertainties correspond to the respecting mean deviation.

ID	Date of event	Start Time (UT)	Duration (seconds)	Latitude (deg)	Longitude (deg)	Altitude (km
GLM-00	2019-02-01	18:17:09	2.651 ± 0.4907	22.45 ± 0.071	-83.50 ± 0.424	
GLM-01	2019-05-23	16:36:18	0.197 ± 0.0000	24.30 ± 0.000	-101.60 ± 0.849	
GLM-02	2019-07-18	14:30:30	0.058 ± 0.0000	27.20 ± 0.000	-103.15 ± 0.778	
GLM-03	2019-08-10	11:18:48	0.199 ± 0.0757	21.50 ± 0.000	-102.50 ± 0.849	
GLM-04	2019-10-03	07:55:33	0.106 ± 0.0297	25.65 ± 0.071	-96.25 ± 0.778	
GLM-05	2019-10-09	06:08:11	0.103 ± 0.0078	23.60 ± 0.000	-111.95 ± 0.212	
GLM-06	2019-11-16	09:36:04	0.396 ± 0.0134	20.30 ± 0.000	-100.55 ± 0.919	
GLM-07	2019-11-17	15:36:01	0.116 ± 0.0035	31.70 ± 0.000	-117.70 ± 1.131	
GLM-08	2019-11-19	07:57:40	0.097 ± 0.1138	20.00 ± 0.000	-88.40 ± 1.131	
GLM-09	2019-11-26	13:23:20	0.078 ± 0.0290	23.90 ± 0.000	-108.70 ± 0.849	
GLM-10	2019-12-04	09:42:54	0.173 ± 0.0028	31.50 ± 0.000	-113.65 ± 0.919	
GLM-11	2019-12-15	14:50:49	0.127 ± 0.0134	27.70 ± 0.000	-114.10 ± 0.849	
GLM-12	2019-12-29	16:16:35	0.062 ± 0.0134	29.60 ± 0.000	-116.35 ± 0.919	
GLM-13	2020-01-03	14:10:17	0.113 ± 0.0085	30.20 ± 0.000	-117.65 ± 0.919	
GLM-14	2020-01-06	16:39:27	0.118 ± 0.0042	31.40 ± 0.000	-108.20 ± 0.990	
GLM-15	2020-01-15	15:00:33	0.213 ± 0.1351	19.45 ± 0.071	-95.55 ± 0.919	
GLM-16	2020-02-12	09:25:40	0.210 ± 0.0226	18.90 ± 0.000	-93.50 ± 0.849	
GLM-17	2020-03-03	12:33:27	0.062 ± 0.0007	18.25 ± 0.071	-106.35 ± 0.636	
GLM-18	2020-03-31	19:31:52	0.105 ± 0.0573	28.45 ± 0.071	-112.05 ± 0.636	
GLM-19	2020-04-08	16:25:28	0.120 ± 0.0926	26.10 ± 0.000	-93.90 ± 0.849	
GLM-20	2020-04-18	17:43:25	0.139 ± 0.0106	29.00 ± 0.000	-106.55 ± 0.919	
GLM-21	2020-04-20	16:05:22	0.318 ± 0.1655	28.15 ± 0.071	-97.85 ± 1.061	
GLM-22	2020-04-25	11:03:09	0.323 ± 0.0813	32.15 ± 0.071	-111.60 ± 1.131	
GLM-23	2020-04-28	19:31:52	0.105 ± 0.0573	28.45 ± 0.071	-112.05 ± 0.636	
GLM-24	2020-05-08	10:06:16	0.490 ± 0.0750	21.60 ± 0.000	-92.40 ± 0.849	
GLM-25	2020-07-15	19:58:28	0.693 ± 0.0495	24.00 ± 0.000	-108.35 ± 0.495	
GLM-26	2020-08-07	13:29:57	0.163 ± 0.0057	28.80 ± 0.000	-106.05 ± 0.919	
GLM-27	2020-09-13	16:41:59	0.184 ± 0.0078	28.45 ± 0.071	-113.75 ± 0.919	
GLM-28	2020-09-30	12:28:11	0.100 ± 0.0078	24.90 ± 0.000	-110.90 ± 0.849	
GLM-29	2020-11-16	12:28:11	0.100 ± 0.0078	24.90 ± 0.000	-110.90 ± 0.849	1
GLM-30	2020-11-17	12:53:41	0.404 ± 0.0262	23.00 ± 0.000	-102.45 ± 0.919	
GLM-31	2020-12-19	10:18:14	0.407 ± 0.0110	21.95 ± 0.071	-101.60 ± 0.990	
GLM-32	2020-12-23	09:43:01	0.148 ± 0.0014	25.75 ± 0.071	-111.25 ± 0.778	
GLM-33	2020-12-29	15:20:54	0.118 ± 0.0014	16.80 ± 0.000	-102.20 ± 0.707	
GLM-34	2021-03-31	09:01:17	0.753 ± 0.3083	20.15 ± 0.071	-92.95 ± 0.212	
GLM-Ven	2019-06-22	21:25:45	4.873 ± 0.0000	14.9 ± 0.000	-65.8 ± 0.000	

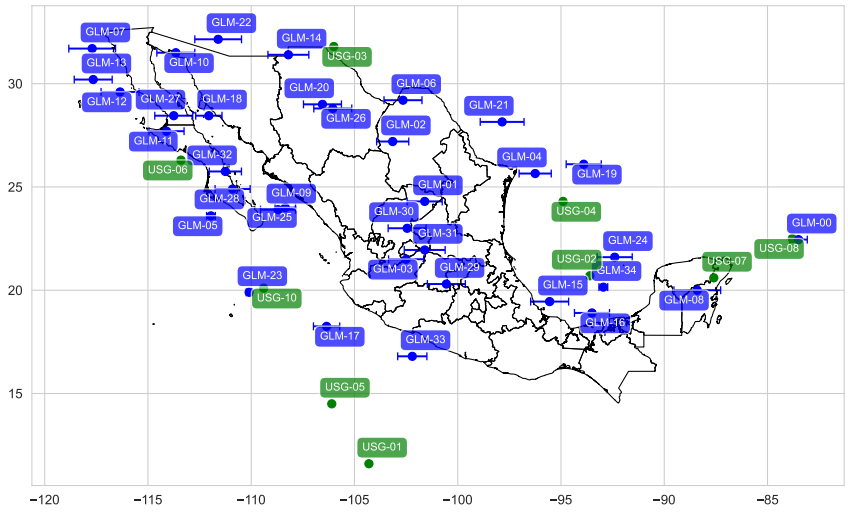

Figure 1. Positions of events from table 1 (blue) and table 2. The events GLM-00/USG-08 actually correpond to the same bolide, but there are little discrepancies about the position where the bolide was detected. The same applies for the events GLM-23/USG-10 and GLM-Ven/USG-09, which not appears in the map.

Table 2. List of bolides detected in mexican territory (plus one detected near Venezuela and one detected near Cuba), detected by USG sensors.

ID	Date of event	Start Time (UT)	Velocity (km/s)				Latitude (deg)	Longitude (deg)	Altitud
			v	v_x	v_y	v_z			
USG-01	1995-08-05	17:14:10					11.6	-104.3	
USG-02	1996-07-12	14:04:45					20.7	-93.6	
USG-03	1997-10-09	18:47:15					31.8	-106.0	
USG-04	2000-01-18	08:33:58					24.3	-94.9	
USG-05	2000-08-25	01:12:25					14.5	-106.1	
USG-06	2005-11-15	05:19:07					26.3	-113.4	
USG-07	2015-07-19	07:06:26	17.8	9.4	13.0	7.8	20.6	-87.6	
USG-08	2019-02-01	18:17:10	16.3	-2.4	13.6	8.7	22.5	-83.8	
USG-09	2019-06-22	21:25:48	14.9	-13.4	6.0	2.5	14.9	-66.2	
USG-10	2020-04-28	05:43:17					20.1	-109.4	

USG sample, the total energy of each meteor is already available from the database, but the energy for GLM bolides needs to be estimated. To do so, we estimated the distance between GOES satellites and the bolide and then followed Jenniskens *et al.* [14], but we find some discrepancies in our measurements repect what is already reported for the same bolides in the USG database. (see the appendix **??** and **??**) for more details. We assumed that such discrepancy is due that GLM detectors underestimate the radiated energy by the bolides since before fragmentation the bolides remain undetectable by GLM sensors, and thus a fraction of the radiated energy is not accounted. To solve this, we estimated a correction factor using the bolides that appears in both GLM and USG samples (see figure **??** in appendix **??**). The energy distributions of USG and GLM samples are compared directly in figure 2.

2.2. GPS data

We got RINEX data from 3 to 7 stations depending of the event location and data availability that surround the event place in all directions as possible. A list of the stations where we got RINEX data is available in table. Most of the stations lie in mexican territory, but in some cases we required data from other stations to cover events near the mexican frontier at north or south.

The obtained RINEX files are compressed in Hatanaka format, developed at the Geographical Survey Institute by Y. Hatanaka [16]. From this files we may estimate the Slant Total Electron Content (sTEC) and the Vertical Total Electron Content (vTEC) which may be computed in the following way:

The Total Electron content along the integrated path of the link (s_i) at the frequency f_i can be inferred from the phase delay L_i of the frequency f_i [17]:

$$L_i = s_i - \frac{40.3082\,\mathrm{m^3\,s^{-1}}}{f_i^2} sTEC_i \tag{1}$$

Combining two observations at two different frequencies f_1 and f_2 we may obtain two different phase delays L_1 and L_2 and derive the TEC along the signal path:

$$sTEC = \frac{f_1^2 f_2^2 (L_1 - L_2)}{40.3082\,\mathrm{m^3\,s^{-1}}(f_1^2 - f_2^2)} \tag{2}$$

In the other hand, the Vertical Total Electron Content (vTEC) is computed from the sTEC as follows [16]:

$$vTEC = \frac{sTEC - [b_R + b_S]}{S(\theta_I)} \tag{3}$$

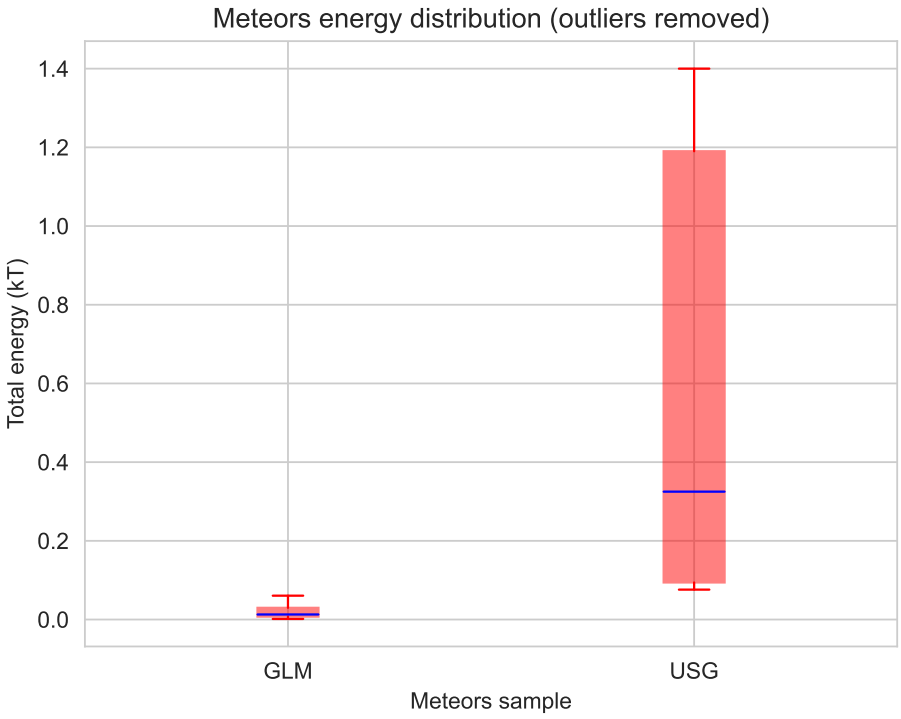

Figure 2. Comparison between released energies of bolides detected by the Geostationary Lightning Mapper and USG sensors.

where b_R and b_S are receiver and satellite biases, respectively. θ_I is the elevation angle in degrees, $S(\theta_I)$ is the obliquity factor with zenith angle ψ at the Ionospheric Pierce Point (IPP):

$$S(\theta_i) = \frac{1}{\cos\psi} = \left\{1 - \frac{R_E \cos\theta_I}{R_E + h}\right\}^{-1/2} \tag{4}$$

Where R_E is the Earth radius in km and $h = 350$ km is the ionospheric shell above the earth's surface.

Using a software developed by Gopi K. Seemala, publicly available at https://seemala.blogspot.com/, we computed the slant TEC (TEC) and vertical TEC (vTEC) for a several number of GPS satellites, each one identified with a PseudoRandom Noise code (PRN). An example of such TEC calculations is shown in figure **??**. The behavior of the TEC curve is due to many factors, including the earth's rotation, solar activity, etc. TID's and wave-like features are not as prominent and are difficult to see. So we focused in a time interval close to the moment the bolide was detected, and detrended our time series following **?**] using a Golay-Savitzky filter of order 7. An example of the resulting detrending signal is shown in figure **??**. The resulting time series are adequate for wavelet analysis.

2.3. Wavelet analysis

Wavelet analysis is a powerful tool for analyzing variations of power within a time series [**?**]. For this task we used a Morlet wavelet $\Psi_0(\eta) = \pi^{-1/4} \exp(i\omega_0\eta) \exp(-\eta^2/2)$, where ω_0 is a non-dimensional frequency, usually set to be 6 to satisfy the admissibity condition [**?**] and η is a non-dimensional "time parameter".

With this, the wavelet transform is given by:

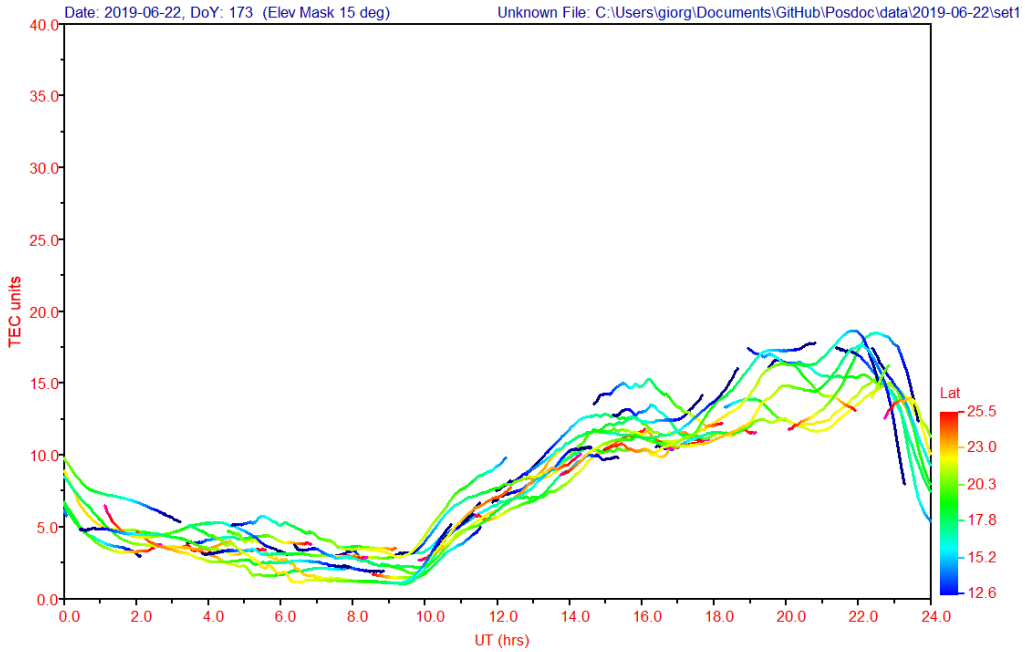

Figure 3. Example of TEC curve obtained for GPS data for the bolide USG-09 from CN05 station.

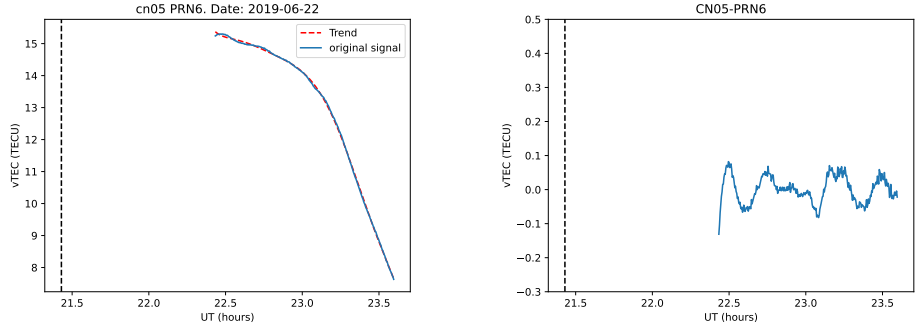

Figure 4. Example of detrending process with USG-09 event. Left: Undetrended TEC series for station CN05 with PRN 6 (blue) versus Golay-Savitsky fit of order 7 (red dashed curve). Right: detrended curve resulting from substracting the Golay-Savitsky fit from the original signal.

$$W_n(s) = \sum_{k=0}^{N-1} \hat{x}_k \hat{\Psi}^*(s\omega_k) \exp(i\omega_k n\delta t) \quad (5)$$

3. Results

%subsectionSubsection

4. Discussion

Authors should discuss the results and how they can be interpreted from the perspective of previous studies and of the working hypotheses. The findings and their implications should be discussed in the broadest context possible. Future research directions may also be highlighted.

5. Conclusions

This section is not mandatory, but can be added to the manuscript if the discussion is unusually long or complex.

6. Patents

This section is not mandatory, but may be added if there are patents resulting from the work reported in this manuscript.

Author Contributions: For research articles with several authors, a short paragraph specifying their individual contributions must be provided. The following statements should be used "Conceptualization, X.X. and Y.Y.; methodology, X.X.; software, X.X.; validation, X.X., Y.Y. and Z.Z.; formal analysis, X.X.; investigation, X.X.; resources, X.X.; data curation, X.X.; writing—original draft preparation, X.X.; writing—review and editing, X.X.; visualization, X.X.; supervision, X.X.; project administration, X.X.; funding acquisition, Y.Y. All authors have read and agreed to the published version of the manuscript.", please turn to the CRediT taxonomy for the term explanation. Authorship must be limited to those who have contributed substantially to the work reported.

Funding: Please add: "This research received no external funding" or "This research was funded by NAME OF FUNDER grant number XXX." and and "The APC was funded by XXX". Check carefully that the details given are accurate and use the standard spelling of funding agency names at https://search.crossref.org/funding, any errors may affect your future funding.

Institutional Review Board Statement: In this section, please add the Institutional Review Board Statement and approval number for studies involving humans or animals. Please note that the Editorial Office might ask you for further information. Please add "The study was conducted according to the guidelines of the Declaration of Helsinki, and approved by the Institutional Review Board (or Ethics Committee) of NAME OF INSTITUTE (protocol code XXX and date of approval)." OR "Ethical review and approval were waived for this study, due to REASON (please provide a detailed justification)." OR "Not applicable" for studies not involving humans or animals. You might also choose to exclude this statement if the study did not involve humans or animals.

Informed Consent Statement: Any research article describing a study involving humans should contain this statement. Please add "Informed consent was obtained from all subjects involved in the study." OR "Patient consent was waived due to REASON (please provide a detailed justification)." OR "Not applicable" for studies not involving humans. You might also choose to exclude this statement if the study did not involve humans.

Written informed consent for publication must be obtained from participating patients who can be identified (including by the patients themselves). Please state "Written informed consent has been obtained from the patient(s) to publish this paper" if applicable.

Data Availability Statement: In this section, please provide details regarding where data supporting reported results can be found, including links to publicly archived datasets analyzed or generated during the study. Please refer to suggested Data Availability Statements in section "MDPI Research Data Policies" at https://www.mdpi.com/ethics. You might choose to exclude this statement if the study did not report any data.

Acknowledgments: In this section you can acknowledge any support given which is not covered by the author contribution or funding sections. This may include administrative and technical support, or donations in kind (e.g., materials used for experiments).

Conflicts of Interest: Declare conflicts of interest or state "The authors declare no conflict of interest." Authors must identify and declare any personal circumstances or interest that may be perceived as inappropriately influencing the representation or interpretation of reported research results. Any role of the funders in the design of the study; in the collection, analyses or interpretation of data; in the writing of the manuscript, or in the decision to publish the results must be declared in this section. If there is no role, please state "The funders had no role in the design of the study; in the collection, analyses, or interpretation of data; in the writing of the manuscript, or in the decision to publish the results".

Sample Availability: Samples of the compounds ... are available from the authors.

Abbreviations

The following abbreviations are used in this manuscript:

MDPI	Multidisciplinary Digital Publishing Institute
DOAJ	Directory of open access journals
TLA	Three letter acronym
LD	Linear dichroism

Appendix A

Appendix A.1

The appendix is an optional section that can contain details and data supplemental to the main text—for example, explanations of experimental details that would disrupt the flow of the main text but nonetheless remain crucial to understanding and reproducing the research shown; figures of replicates for experiments of which representative data are shown in the main text can be added here if brief, or as Supplementary Data. Mathematical proofs of results not central to the paper can be added as an appendix.

Table A1. This is a table caption.

Title 1	Title 2	Title 3
Entry 1	Data	Data
Entry 2	Data	Data

Appendix B

All appendix sections must be cited in the main text. In the appendices, Figures, Tables, etc. should be labeled, starting with "A"—e.g., Figure A1, Figure A2, etc.

References

1. Blanco-Cano, X.; Omidi, N.; Russel, C.T. How to make a magnetosphere. *Astronomy & Geophysics* **2004**, *45*, 3.14–3.17. doi:10.1046/j.1468-4004.2003.45314.x.
2. Zolesi, B.; Cander, L.R. *Ionospheric Prediction and Forecasting*; Springer Geophysics, 2014.
3. Cnossen, I.; Wiltberger, M.; Ouellette, J.E. The effects of seasonal and diurnal variations in the Earth's magnetic dipole orientation on solar wind–magnetosphere-ionosphere coupling. *Journal of Geophysical Research: Space Physics* **2012**, *117*. doi:https://doi.org/10.1029/2012JA017825.
4. Vázquez, M.; Vaquero, J.M.; Gallego, M.C.; Roca Cortés, T.; Pallé, P.L. Long-Term Trends and Gleissberg Cycles in Aurora Borealis Records (1600 - 2015). **2016**, *291*, 613–642. doi:10.1007/s11207-016-0849-6.
5. Oka, M.; Phan, T.D.; Eastwood, J.P.; Angelopoulos, V.; Murphy, N.A.; Øieroset, M.; Miyashita, Y.; Fujimoto, M.; McFadden, J.; Larson, D. Magnetic reconnection X-line retreat associated with dipolarization of the Earth's magnetosphere. *Geophysical Research Letters* **2011**, *38*. doi:https://doi.org/10.1029/2011GL049350.
6. Vlasov, M.N.; Kelley, M.C. Crucial discrepancy in the balance between extreme ultraviolet solar radiation and ion densities given by the international reference ionosphere model. *Journal of Geophysical Research: Space Physics* **2010**, *115*. doi:https://doi.org/10.1029/2009JA015103.

7. Helmboldt, J.F.; Lane, W.M.; Cotton, W.D. Climatology of midlatitude ionospheric disturbances from the Very Large Array Low-frequency Sky Survey. *Radio Science* **2012**, *47*. doi:https://doi.org/10.1029/2012RS005025.
8. Chilcote, M.; LaBelle, J.; Lind, F.D.; Coster, A.J.; Miller, E.S.; Galkin, I.A.; Weatherwax, A.T. Detection of traveling ionospheric disturbances by medium-frequency Doppler sounding using AM radio transmissions. *Radio Science* **2015**, *50*, 249–263. doi:https://doi.org/10.1002/2014RS005617.
9. Rodríguez-Martínez, M.; Pérez-Enríquez, H.R.; Carrillo-Vargas, A.; López-Montes, R.; Araujo-Pradere, E.A.; Casillas-Pérez, G.A.; Cruz-Abeyro, J.A.L. Ionospheric Disturbances and Their Impact on IPS Using MEXART Observations. **2014**, *289*, 2677–2695. doi:https://doi.org/10.1007/s11207-014-0496-8.
10. Lin, C.H.; Lin, J.T.; Chen, C.H.; Liu, J.Y.; Sun, Y.Y.; Kakinami, Y.; Matsumura, M.; Chen, W.H.; Liu, H.; Rau, R.J. Ionospheric shock waves triggered by rockets. *Annales Geophysicae* **2014**, *32*, 1145–1152. doi:10.5194/angeo-32-1145-2014.
11. Yang, Y.M.; Komjathy, A.; Langley, R.B.; Vergados, P.; Butala, M.D.; Mannucci, A.J. The 2013 Chelyabinsk meteor ionospheric impact studied using GPS measurements. *Radio Science* **2014**, *49*, 341–350. doi:https://doi.org/10.1002/2013RS005344.
12. Sergeeva, M.A.; Demyanov, V.V.; Maltseva, O.A.; Mokhnatkin, A.; Rodriguez-Martinez, M.; Gutierrez, R.; Vesnin, A.M.; Gatica-Acevedo, V.J.; Gonzalez-Esparza, J.A.; Fedorov, M.E.; et al. Assessment of Morelian Meteoroid Impact on Mexican Environment. *Atmosphere* **2021**, *12*. doi:10.3390/atmos12020185.
13. Goodman, S.J.; Blakeslee, R.J.; Koshak, W.J.; Mach, D.; Bailey, J.; Buechler, D.; Carey, L.; Schultz, C.; Bateman, M.; McCaul, E.; et al. The GOES-R Geostationary Lightning Mapper (GLM). *Atmospheric Research* **2013**, *125-126*, 34–49. doi:https://doi.org/10.1016/j.atmosres.2013.01.006.
14. Jenniskens, P.; Albers, J.; Tillier, C.E.; Edgington, S.F.; Longenbaugh, R.S.; Goodman, S.J.; Rudlosky, S.D.; Hildebrand, A.R.; Hanton, L.; Ciceri, F.; et al. Detection of meteoroid impacts by the Geostationary Lightning Mapper on the GOES-16 satellite. *Meteoritics & Planetary Science* **2018**, *53*, 2445–2469. doi:https://doi.org/10.1111/maps.13137.
15. Rumpf, C.M.; Longenbaugh, R.S.; Henze, C.E.; Chavez, J.C.; Mathias, D.L. An Algorithmic Approach for Detecting Bolides with the Geostationary Lightning Mapper. *Sensors* **2019**, *19*. doi:10.3390/s19051008.
16. Kumar, D.S.; Priyadarshi, S.; Seemala, G.; Singh, A. GPS-TEC variations during low solar activity period (2007-2009) at Indian low latitude stations. *Astrophysics and Space Science* **2012**, *339*, 165–178. doi:10.1007/s10509-011-0973-6.
17. Emery, W.; Camps, A. Chapter 6 - Remote Sensing Using Global Navigation Satellite System Signals of Opportunity. In *Introduction to Satellite Remote Sensing*; Emery, W.; Camps, A., Eds.; Elsevier, 2017; p. 455–564. doi:10.1016/B978-0-12-809254-5.00006-3.